Atomic photoionization in a strong magnetic field

Chris H. Greene
Department of Physics and Astronomy, Louisiana State University, Baton Rouge, Louisiana 70803
(Received 22 April 1983)

The photoionization of hydrogen atoms in a strong magnetic field is formulated as a multichannel problem by representing the asymptotic electron wave function in cylindrical coordinates. Departures from cylindrical symmetry close to the nucleus are incorporated by an R-matrix treatment at short range, which then merges with standard quantum-defect procedures. The R-matrix calculation utilizes the eigenchannel approach, recast in noniterative form. At the field strength treated here, $B=4.7\times10^9$ G, the photoionization cross section displays narrow "autoionizing" resonances near the excited Landau thresholds.

I. INTRODUCTION

Magnetic white dwarfs exhibit field strengths approaching 10^9 G, and so the interpretation of white-dwarf spectra requires a detailed understanding of atomic properties in such fields.[1] Also, the quantum-mechanical motion of an electron in combined Coulomb and magnetic fields constitutes one of the simplest nonseparable problems in atomic physics; its properties have fundamental implications for the physics of all correlated systems.[2,3] While for certain atomic properties the Hamiltonian appears to be quasiseparable,[4,5] for other properties the nonseparability becomes paramount, e.g., the decay of quasi-Landau levels observed at smaller fields,[6] or the "autoionization" of states lying below excited Landau thresholds.[7,8]

In the discrete spectrum much attention has been given to the problem of calculating energy levels and oscillator strengths (see, e.g., Ref. 9). The most complete and accurate results, obtained over a wide range of field strengths, appear to be those of Wunner and Ruder.[10] Photoionization of hydrogen in strong fields was treated by Kara and McDowell,[11] though many aspects of their calculation are unrealistic because of an inadequate treatment of Coulomb field effects at the Landau thresholds. At much higher fields ($B\sim10^{12}$ G) than considered here, a realistic calculation of the photoionization cross section was obtained by Wunner *et al.*,[12] though the "autoionizing" resonances were not included. The energies and widths of several autoionizing states were calculated by Friedrich and Chu,[7] and scattering amplitudes were obtained by Onda,[8] though the photoionization cross section was not given.

The central purpose of this paper is the presentation of a multichannel R-matrix calculation of the photoionization cross section for hydrogen. For this prototype calculation only a single value of the magnetic field (4.7×10^9 G) and of the photon polarization ($\hat{\epsilon}||\vec{B}$) will be considered. The escape of the photoelectron to $z\rightarrow\pm\infty$ is conveniently represented here in terms of regular and irregular Coulomb wave functions, whereby the standard results of quantum-defect theory[13–17] suffice to translate the short-range R-matrix calculation into a photoionization cross section. Clark[18] has recently developed a closely related approach to treat negative-ion photodetachment in a magnetic field.

A second objective of this study is to test the feasibility of a noniterative reformulation of the eigenchannel R-matrix approach,[19] which amounts to a generalization of the variational expression derived by Kohn[20] for the logarithmic derivative of the wave function at a finite radius. This version of R-matrix theory is closely related to that described by Taylor,[21] Lane and Robson,[22] Purcell and Chatwin,[23] and Oberoi and Nesbet.[24] A new application of the same approach to molecular dynamics is described by Rouzo and Raseev.[25] The results of the calculation, given in Sec. III, show how the short-range reaction matrix varies strongly as the energy is increased from far below a threshold up to the near-threshold region. The reaction matrix, nonetheless, becomes a smooth function of the energy once E is within a few electron volts of an opening threshold. These results complement an earlier study of this energy dependence in a much different context.[26]

II. NONITERATIVE CALCULATION OF R-MATRIX EIGENSTATES

In the interest of keeping this paper self-contained, the noniterative eigenchannel R-matrix method will be derived in this section. This method retains the rapid convergence of the eigenchannel approach[19,27] while eliminating its main disadvantage, namely, the necessity for iteratively diagonalizing the Hamiltonian several times at each energy. It is closely related to the noniterative approach developed by Refs. 21–24, with the main difference being the present emphasis on R-matrix *eigenstates* rather than on the full R matrix. The motivation for focusing on these eigenstates stems from their having a simple physical interpretation in many problems.[14,28]

The common thread in all R-matrix methods[29] is their solution of the Schrödinger equation within a finite reaction volume Ω of configuration space. The scattering properties of a many-particle system are known once the normal logarithmic derivative $(\partial\psi/\partial n)\psi^{-1}$ is specified on the surface Σ enclosing the reaction volume. The goal of

theory is to determine this information in the form of an R matrix.

Consider the Ritz variational expression for the Schrödinger energy eigenvalue

$$E=\frac{\int_\Omega \psi^*(-\frac{1}{2}\nabla^2\psi+V\psi)d\omega}{\int_\Omega \psi^*\psi\, d\omega}\ , \tag{1}$$

where $d\omega$ is the differential volume element of configuration space and the integrals extend only over the reaction volume Ω. (In a many-particle system, ∇^2 must be interpreted as $\sum_i \nabla_i^2/m_i$.) Application of Green's theorem transcribes Eq. (1) into

$$E=\frac{\int_\Omega(\frac{1}{2}\vec{\nabla}\psi^*\cdot\vec{\nabla}\psi+\psi^*V\psi)d\omega-\frac{1}{2}\int_\Sigma\psi^*(\partial\psi/\partial n)d\sigma}{\int_\Omega\psi^*\psi\, d\omega}\ , \tag{2}$$

in which an additional integral must now be evaluated over the surface Σ of the reaction volume. The differential area element is $d\sigma$, and the normal derivative $\partial\psi/\partial n$ on Σ can be expressed in terms of ψ and the constant b through

$$\frac{\partial\psi}{\partial n}+b\psi=0\ , \tag{3}$$

on Σ. [In a multichannel problem having several degenerate continuum solutions, Eqs. (2) and (3) are meant to hold for each independent solution ψ_β with its associated constant b_β. It is worth emphasizing that b in Eq. (3) is not necessarily a constant for any arbitrary state ψ. Yet we can always look for the set of R-matrix eigenstates ψ_β for which b_β *is* a constant on Σ, in which case b_β is interpreted as an eigenvalue of the R-matrix.] Consequently, the expression (2) can be written in a form more useful for continuum states at a given energy E, as an equation for the unknown $b(E)$:

$$b=\frac{\int_\Omega[-\vec{\nabla}\psi^*\cdot\vec{\nabla}\psi+2\psi^*(E-V)\psi]d\omega}{\int_\Sigma\psi^*\psi\, d\sigma}\ . \tag{4}$$

This expression for b is clearly real and, moreover, the first variation δb vanishes to first order in small deviations $\delta\psi$ of the wave function from the exact solution ψ. This stationary property follows upon evaluating δb using Eq. (4) and then applying Green's theorem. Importantly, *no constraint* needs to be imposed on the trial functions in showing that $\delta b=0$. In particular, the trial functions need not have any specified logarithmic derivative on the reaction surface Σ. In this sense Eq. (4) is a less restrictive variational expression than Eq. (1), since the *energy* functional is stationary only when all trial functions have the same normal logarithmic derivative on Σ as the exact solution.

A. Generalized eigenvalue problem for the R-matrix eigenstates

A particularly convenient method for using Eq. (4) to calculate the R-matrix follows from using trial functions which are a linear combination of basis functions y_k:

$$\psi=\sum_k c_k y_k\ . \tag{5}$$

In the following, the c_k, y_k, and ψ will be assumed real without loss of generality, as the Hamiltonian is real. It should be pointed out that the y_k need not be orthogonal, and also they need not have any particular logarithmic derivative on Σ; indeed their normal logarithmic derivatives should ideally span a range of values. Equation (4) then takes the form

$$b[c_k]=\sum_{k,l}c_k\Gamma_{kl}c_l\Big/\sum_{k',l'}c_{k'}\Lambda_{k'l'}c_{l'}\ . \tag{6}$$

The real symmetric matrices $\underline{\Gamma}$ and $\underline{\Lambda}$ are defined by

$$\Gamma_{kl}=\int_\Omega[-\vec{\nabla}y_k\cdot\vec{\nabla}y_l+2y_k(E-V)y_l]d\omega\ , \tag{7}$$

$$\Lambda_{kl}=\int_\Sigma y_k y_l d\sigma\ . \tag{8}$$

The element Γ_{kl} can also be put in the more conventional form involving the matrix element of a non-Hermitian Hamiltonian and a surface term

$$\Gamma_{kl}=2\int_\Omega y_k(E-H)y_l d\omega-\int_\Sigma y_k\frac{\partial y_l}{\partial n}d\sigma\ . \tag{9}$$

A necessary condition for b to be stationary with respect to small variations of the c_k is that

$$\frac{\partial b}{\partial c_k}=0=\left[\sum_{k',l'}c_{k'}\Lambda_{k'l'}c_{l'}\right]^{-1}\left[\sum_l\Gamma_{kl}c_l-b\sum_l\Lambda_{kl}c_l\right]\ . \tag{10}$$

In matrix notation this amounts to the generalized eigenvalue equation

$$\underline{\Gamma}\vec{c}=b\underline{\Lambda}\vec{c}\ . \tag{11}$$

Properties of the eigensystem (11) are discussed in Ref. 30, and an algorithm for numerical solution which appears to be stable and efficient is presented in Refs. 31 and 32. Eigenvectors $\vec{c}_\beta$ and $\vec{c}_{\beta'}$ corresponding to distinct eigenvalues b_β and $b_{\beta'}$ are orthogonal over the reaction surface Σ:

$$\vec{c}_{\beta'}\cdot\underline{\Lambda}\vec{c}_{\beta'}=0\ , \tag{12}$$

when $b_\beta\neq b_{\beta'}$. The number of nontrivial solutions to Eq. (11) depends on the problem being studied. On physical grounds the number of eigensolutions must equal the number of open and weakly closed channels, which amounts to those reaction channels having non-negligible amplitude on Σ. The remaining channels, which may contribute at short range but are exponentially small on Σ, are referred to as strongly closed.

The concept of reaction channels arises here by introducing a complete set of real orthonormal surface harmonics ϕ_n which span the surface Σ:

$$\int_\Sigma\phi_n\phi_{n'}d\sigma=\delta_{nn'}\ . \tag{13}$$

Each of the basis functions y_k can be expanded in terms of the ϕ_n over Σ according to

$$y_k=\sum_n a_{kn}\phi_n\ , \tag{14}$$

on Σ, and the matrix elements of $\underline{\Lambda}$ are then simply

$$\Lambda_{kl}=\sum_n a_{kn}a_{ln} \ . \tag{15}$$

If Γ and Λ are $n\times n$ matrices and Λ is nonsingular, then there are n nontrivial solutions to Eq. (11). In practice, however, Λ is highly singular because only a few terms (i.e., *channels)* contribute to the summation in (15). In the extreme case of a single-channel problem, the matrix Λ is factorable and thus has but one nonzero eigenvalue, whereby the system (11) has exactly one nontrivial solution at each energy, as expected. Similarly, if a total of N channels are required to span the reaction surface Σ at any given energy, then the number of relevant eigensolutions is also N. Besides the eigenvalues b_β, the R-matrix eigenvectors are also required to construct the matrix $\underline{R}$. In the present formulation these R-matrix eigenvectors are (within normalization) the projection of the β'th eigensolution

$$\psi_\beta=\sum_k y_k c_{k\beta} \tag{16}$$

onto the n'th surface harmonic

$$\begin{aligned} Z_{n\beta}&=\int_\Sigma \phi_n\psi_\beta d\sigma/N_\beta \\ &=\sum a_{kn}c_{k\beta}/N_\beta \ , \end{aligned} \tag{17}$$

with the normalization constant given by

$$N_\beta^2=\sum_n\left[\int_\Sigma \phi_n\psi_\beta d\sigma\right]^2 . \tag{18}$$

Finally, the R matrix is given by

$$R_{nn'}=\sum_\beta Z_{n\beta}b_\beta Z_{n'\beta} \ , \tag{19}$$

which is automatically symmetric.

Whereas testing the symmetry of the R matrix provides a useful check on convergence for some methods of calculation, it is of no value in the present approach since $\underline{R}$ in (19) is automatically symmetric. One useful test of convergence is the comparison of b_β obtained from (11) with the value obtained from the less-accurate expression

$$b_{\beta,\text{approx}}=-\frac{\int_\Sigma \psi_\beta(\partial\psi_\beta/\partial n)d\sigma}{\int_\Sigma \psi_\beta^2 d\sigma} \ , \tag{20}$$

calculated using the variational wave function ψ_β. Since Eq. (20) differs from the exact b_β in first order ($\delta\psi$), while Eq. (11) differs in second order ($\delta\psi^2$), their difference measures the convergence of the expansion (5).

B. Photoionization in a magnetic field

Next, the specific application of R-matrix theory to treat the photoionization of hydrogen in a strong field is addressed. In cylindrical coordinates the Hamiltonian is (in a.u.)

$$\begin{aligned} H=&-\frac{1}{2}\frac{\partial^2}{\partial\rho^2}-\frac{1}{2\rho}\frac{\partial}{\partial\rho}-\frac{1}{2}\frac{\partial^2}{\partial z^2}+\frac{L_z^2}{2\rho^2}+\alpha L_z+\tfrac{1}{2}\alpha^2\rho^2 \\ &-(\rho^2+z^2)^{-1/2} \ , \end{aligned} \tag{21}$$

where $\alpha\equiv eB/2m_ec$ is the Larmor frequency. As is well known, this Hamiltonian is approximately separable in spherical coordinates at short distances ($r\lesssim r_c$), but is nearly separable in cylindrical coordinates farther out ($r\gtrsim r_c$). If the electron kinetic energy is roughly T, then this critical radius lies in the neighborhood of $r_c\approx(2T)^{1/2}\alpha^{-1}$ bohr radii. The photoelectron can escape beyond this distance only by moving parallel to the magnetic field, and its kinetic energy of escape depends on the azimuthal quantum number m and on the asymptotic Landau quantum number n characterizing the motion in ρ. To account properly for this channel structure the asymptotic wave function in a photoionization calculation *must* be expressed in cylindrical coordinates even for relatively weak fields. Notice also that for large $|z|\gg r_c$, the potential energy assumes the form $-1/|z|$. Hence, each Landau component of ψ can be written as a linear combination of regular and irregular Coulomb functions (f,g) in z. This feature permits the use of multichannel quantum-defect theory[15,17] to express the photoionization cross section in terms of a short-range reaction matrix and dipole matrix elements, all of which vary smoothly with energy.

In the terminology of Sec. II A, then, the reaction surface Σ is cylindrical, with the ends of the cylinder taken to be

$$z=\pm z_0 \ . \tag{22}$$

The actual value of z_0 will depend on the energy range and on the magnetic field in general. The radius of the cylinder ρ_0 need not be specified here since the electron can escape only a finite distance in ρ at any given energy. Thus, ρ_0 will simply be imagined large enough to contain all possible excitations in ρ. The natural choice for the surface harmonics in this problem are the wave functions associated with the Landau levels of a free electron in a magnetic field:

$$\phi_n^{(m)}(\rho,\phi)\equiv N_{nm}e^{im\phi}e^{-\alpha\rho^2/2}(\alpha\rho^2)^{|m|/2}L_n^{(|m|)}(\alpha\rho^2) \ , \tag{23}$$

with an associated residual channel-energy level

$$E_n^{(m)}=\alpha(2n+|m|+m+1) \ . \tag{24}$$

Here N_{nm} is a normalization constant and $L_n^{(|m|)}$ is an associated Laguerre polynomial.

As quantum-defect procedures have been described elsewhere, relevant details will only be summarized here. The key point is that solutions to the Schrödinger equation at $|z|\geq z_0$ can be represented in terms of regular and irregular Coulomb wave functions f_n and g_n. In the present problem f_n and g_n are the $l=0$ energy-normalized base pair of Refs. 15–17 evaluated at the appropriate channel energy

$$\epsilon_n^{(m)}=E-E_n^{(m)} \ , \tag{25}$$

which can be positive or negative. The explicit form of the β'th independent solution of Eq. (11) can thus be written in terms of constants $I_{n\beta}$ and $J_{n\beta}$ as

$$\psi_\beta=\sum_n\phi_n^{(m)}(\rho,\phi)[f_n(z)I_{n\beta}-g_n(z)J_{n\beta}], \quad z\geq z_0 \ . \tag{26}$$

As each ψ_β is either even or odd about $z=0$, it suffices to consider the region $z \geq z_0$ only.[33] The coefficients $I_{n\beta}$ and $J_{n\beta}$ are found by projecting each ψ_β onto $\psi_n^{(m)}$, as well as its normal derivative

$$\frac{\partial \psi_\beta}{\partial z} = -b_\beta \psi_\beta = \sum_n \phi_n^{(m)}(\rho,\phi)[f_n'(z) I_{n\beta} - g_n'(z) J_{n\beta}], \quad z \geq z_0 \tag{27}$$

and solving the resulting linear system after setting $z=z_0$. The coefficients $I_{n\beta}$ and $J_{n\beta}$ define the reaction matrix $K_{nn'}$ through

$$\underline{K} = \underline{J}\,\underline{I}^{-1}, \tag{28}$$

though it is useful in practice to deal separately with the reaction matrix eigenvalues $\tan\pi\mu_\alpha$ and eigenvectors $U_{n\alpha}$ by solving

$$\underline{K}\,\underline{U} = \underline{U}\tan(\pi\underline{\mu}) . \tag{29}$$

The eigenstates of the short-range reaction matrix will be denoted Ψ_α; these are linear combinations of the R-matrix eigenstates ψ_β:

$$\Psi_\alpha = \sum_{\beta n} \psi_\beta (\underline{I}^{-1})_{\beta n} U_{n\alpha} \cos(\pi\mu_\alpha) . \tag{30}$$

The Ψ_α have the standard asymptotic form

$$\Psi_\alpha = \sum_n \phi_n^{(m)}(\rho,\phi)[f_n(z) U_{n\alpha}\cos(\pi\mu_\alpha) - g_n(z) U_{n\alpha}\sin(\pi\mu_\alpha)], \quad z \geq z_0 . \tag{31}$$

Photoabsorption depends lastly on the dipole matrix elements between[33] Ψ_α and Ψ_0, the ground-state wave function

$$d_\alpha = \int_0^{2\pi} d\phi \int_0^\infty \rho\, d\rho \int_0^\infty dz\, \Psi_\alpha^*(\rho,\phi,z)\hat{\epsilon}\cdot\vec{r}\,\Psi_0(\rho,\phi,z) . \tag{32}$$

The d_α, μ_α, and $U_{n\alpha}$ determine the total and partial photoionization cross sections, as detailed in Ref. 17. These parameters are smooth functions of energy (as seen in Sec. III), even through ionization thresholds. This fact allows them to be calculated on a coarse mesh of energies, even though the cross section itself changes rapidly with energy.

III. PROTOTYPE CALCULATION

The R-matrix procedure discussed above has been implemented at one value of the magnetic field, $B = 4.7\times10^9$ G, corresponding to $\alpha = 1$ in Eq. (21). It has also been limited to incident photons which are linearly polarized along the field axis $\hat{z}$, thereby selecting only the $m=0$, odd-parity final state. The main elements required for a realistic calculation can be discerned from Fig. 1, which shows the diagonal potential matrix elements for $m=0$ and $\alpha=1$:

$$V_{nn}(z) = E_n^{(0)} - \int_0^\infty \rho\, d\rho \int_0^{2\pi} d\phi\, |\phi_n^{(0)}(\rho,\phi)|^2 \times(\rho^2+z^2)^{-1/2} , \tag{33}$$

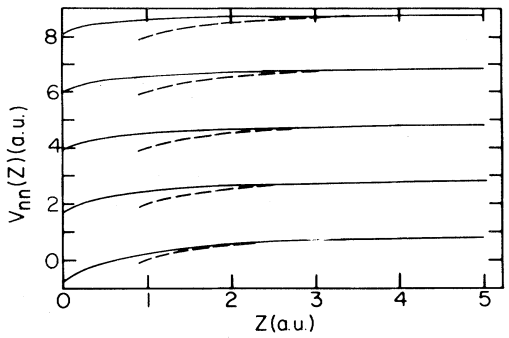

FIG. 1. Diagonal potential matrix elements which are given by Eq. (33), converging to the lowest five Landau levels as $|z| \to \infty$. These are the potentials relevant for $m=0$, at a magnetic field 4.7×10^9 G. Also shown as dashed curves are the purely Coulombic potentials $-1/|z|$ converging to each Landau level.

where $E_n^{(0)} = \alpha(2n+1)$ and $n=0$, 1, etc. These integrals were found numerically using Simpson's rule, except at $z=0$ where they could be evaluated simply in closed form. Of course, their convergence to the asymptotic form

$$V_{nn}(z) \xrightarrow[|z|\to\infty]{} \alpha(2n+1) - 1/|z| + O(|z|^{-3}) \tag{34}$$

is slower for high n because $\langle\rho\rangle$ is correspondingly larger and (34) is satisfied only for $|z| \gg \langle\rho\rangle$. Figure 1 demonstrates that for energies up to a few a.u. a choice for the R-matrix boundary of $z_0=5$ a.u. should easily suffice. Inspection of the off-diagonal terms of the potential matrix confirms that they are negligible at $z_0=5$ a.u.

The calculation of the $m=0$, even-parity ground state is perfomed at only one energy. Rather than using the R-matrix approach, it is therefore more convenient to diagonalize the Hamiltonian in an orthonormal basis set which vanishes at $|z| \geq z_0 = 5$ a.u. and has a vanishing z derivative at $z=0$. The basis set of 23 functions which was used is (for $|z| < z_0$)

$$y_{nj}(\rho,\phi,z) = \begin{cases} \phi_n^{(0)}(\rho,\phi)(2/z_0)^{1/2}\cos[\pi(j-\frac{1}{2})z/z_0], \\ \qquad n=0,1 \text{ and } j=1,\ldots,10 \\ \phi_n^0(\rho,\phi)(8\gamma/\pi)^{1/4}\exp(-\gamma z^2), \quad n=2,3,4 . \end{cases} \tag{35}$$

Matrix elements of H were evaluated numerically using an efficient Filon scheme for integrals involving cosine functions and Simpson's rule for the others.[34] The parameter γ was optimized roughly at the value $\gamma=2.5$ and then held constant. The lowest energy eigenvalue so obtained is $E_0 = -0.002\,38$ a.u., corresponding to a binding energy of 1.0024 a.u. This value is in satisfactory agreement with more sophisticated calculations, e.g., Wunner and Ruder[10] obtain a binding energy of 1.0222 a.u. Figure 2 shows the ground-state wave-function components in each of the Landau channels; it confirms that the higher channels ($n \geq 1$) contribute only at short range.

The $m=0$, odd-parity final state has a node at $z=0$. This fact diminshes the effect of the spherical volume

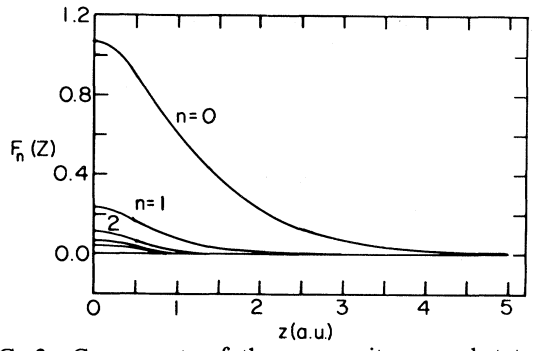

FIG. 2. Components of the even-parity ground-state wave function are shown in the lowest five Landau channels, for $m=0$.

near $r=0$, and implies that the cylindrical expansion should converge more rapidly than it did for the ground state; hence, only the lowest two Landau channels were retained. The variational basis used for the R-matrix calculation is

$$y_{nj}(\rho,\phi,z)=\phi_n^{(0)}(\rho,\phi)\sin(jz/2)\ , \tag{36}$$

with $n=0$ or 1 and $j=1,2,\ldots,j_{\max}$. The final calculation used $j_{\max}=15$, giving a total of 30 nonorthogonal basis functions. Some of the calculations were repeated with $j_{\max}=10$ to assure convergence of the expansion.

For an N-channel problem there are N independent solutions ψ_β obtained by solving the eigenvalue problem (11). It is useful to write these solutions in the form

$$\psi_\beta(\rho,\phi,z)=\sum_n \phi_n^{(0)}(\rho,\phi)F_{n\beta}(z), \quad |z|\geq z_0\ . \tag{37}$$

The R matrix can be calculated from values of $F_{n\beta}(z_0)$ and its derivative with respect to z, $F'_{n\beta}(z_0)$:

$$\underline{R}=-\underline{F}'(z_0)[\underline{F}(z_0)]^{-1}\ . \tag{38}$$

If the ψ_β are eigenstates of the R matrix, then $F'_{n\beta}(z_0)=-b_\beta F_{n\beta}(z_0)$, and $\underline{R}$ is given by

$$R_{nn'}=\sum_\beta F_{n\beta}(z_0)b_\beta[\underline{F}(z_0)^{-1}]_{\beta n'}\ , \tag{39}$$

which is equivalent to Eq. (19). But $\underline{F}'(z_0)$ can also be calculated by explicitly taking the derivative of the variational solution. This gives, in general, a less-accurate R matrix when (38) is evaluated. In Table I the two-channel R matrices calculated at $E=3.1$ a.u. for the $m=0$, odd-parity final state using these two methods are compared. The R matrix found using (39) is denoted "variational"; it is exactly symmetric at all levels of approximation. The less-accurate R matrix found from (38) is denoted "approximate"; its asymmetry $R_{10}-R_{01}$ provides one measure of the inaccuracy of the calculation. The last row of Table I gives the R matrix calculated by direct numerical integration of the two-channel close-coupling equations. Its good agreement with the best variational results (third row of Table I) confirms the accuracy of the calculation.

A. Single-channel regime

At energies below 2.4 a.u. the first excited-channel wave function ($n=1$) has no appreciable amplitude at $|z|=z_0$. This fact reduces the problem to a one-channel situation, even though the excited channel(s) still contribute to Ψ *within* the reaction zone. Throughout this one-channel regime the results of the R-matrix calculation can be summarized by a single-channel quantum defect $\mu_0(E)$ and a single-dipole matrix element $d_0(E)$ connecting the ground state to an energy-normalized final state. In keeping with the quantum-defect point of view, these are calculated as a continuous function of energy even below the $n=0$ ionization threshold at $E_0^{(0)}=1$ a.u. The regular and irregular Coulomb wave functions needed at $z_0=5$ a.u. were evaluated by a power-series expansion. Figure 3 shows the quantum defect throughout this energy range. It varies slowly with energy in general, though below $E=0.8$ a.u., μ_0 begins to vary more rapidly with E, reflecting the presence of the lowest member of the Rydberg series at $E=0.7029$ a.u. The differential oscillator-strength distribution df/dE, calculated using both the length and velocity[35] forms of the dipole matrix element, appears in Fig. 4. This gives the photoionization cross section at $E>1$ a.u. Below that energy the photoabsorption spectrum is entirely discrete, despite the fact that μ_0 and df/dE are shown continuously. The energies of the bound levels are determined by the requirement that

$$\mu_0(E)+\nu_0(E)=P\ , \tag{40}$$

for P integer, where the effective quantum number is

$$\nu_0(E)=[2(E_0^{(0)}-E)]^{-1/2}\ . \tag{41}$$

At those energies satisfying (40) the discrete oscillator strengths are related to df/dE by

$$f_N=(df/dE)_{E_N}/(\nu_0^3+d\mu_0/dE)_{E_N}\ . \tag{42}$$

These bound-state energies and the oscillator strengths connecting to the ground state are compared in Table II

TABLE I. R matrices at $E=3.1$ a.u. as calculated by different methods.

Method	$j_{\max}$	R_{00}	R_{11}	R_{01}	R_{10}
Variational	10	0.969 98	0.117 72	0.165 78	0.165 78
Approximate	10	0.924 03	0.121 98	0.160 74	0.150 99
Variational	15	0.971 17	0.117 78	0.166 03	0.166 03
Approximate	15	0.973 87	0.119 27	0.167 21	0.169 33
Close coupling		0.971 26	0.117 78	0.166 04	0.165 98

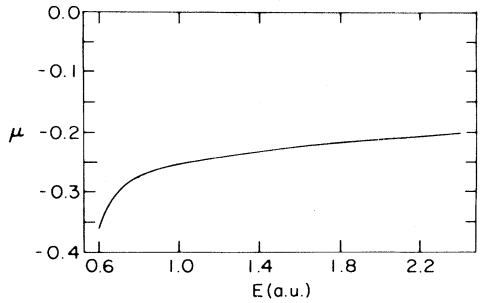

FIG. 3. Single-channel quantum defect ($m=0$, even parity) is shown as a smooth function of energy near the lowest ionization threshold $E_0^{(0)}=1$ a.u.

with the calculation of Refs. 10 and 36. While the agreement is reasonably good, there is a noticeable discrepancy between the length oscillator strengths and the velocity values for all levels but the lowest. The origin of this discrepancy is not fully understood. The oscillator-strength sum, which should be unity, is found to be $\sum f_N=0.954$ (length), $\sum f_N=0.950$ (velocity). These sums include the lowest seven discrete levels, an estimate of the remaining discrete levels, and the continuum up to $E=2.4$ a.u. The discrete spectrum contributes roughly 75% of this sum compared with 56.5% for hydrogen in zero external field.[37]

B. Two-channel regime

The energy range from $E=2.4$—4 a.u., which contains the first excited $m=0$ Landau threshold ($n=1$) at $E_1^{(0)}=3$ a.u., can be treated as a two-channel problem. The 2×2 orthogonal matrix $U_{n\alpha}$ can be parametrized in terms of a mixing angle θ; together with the eigenquantum defects μ_2 and μ_1, these determine the reaction matrix. The two dipole matrix elements d_α were calculated in the dipole length approximation using (32) and in the dipole velocity approximation using an analogous expression. These five smoothly varying short-range parameters are shown as a function of energy in Figs. 5—7. The increasing value of $|\theta/\pi|$ implies a gradual increase in the channel mixing as the energy increases from $E=2.4$ a.u. toward the $n=1$ threshold. This onset of channel mixing is more gradual than that observed in Ref. 26. It is best reflected in the squared off-diagonal scattering matrix element

$$|S_{01}|^2=\sin^2(2\theta)\sin^2[\pi(\mu_1-\mu_2)]\ ,$$

which (for $E>3$ a.u.) can be interpreted as the probability that an ($m=0$, odd-parity) electron incident in the lowest Landau channel will emerge in the first excited channel. Figures 5 and 6 show that $|S_{01}|^2$ increases from the small value 0.004 at $E=2.4$ up to the non-negligible value 0.16 at $E=3.2$. Nonetheless, this implies a relatively small channel mixing throughout this energy range, as expected because of the node at $z=0$ in the final state. In simpler terms, the small mixing suggests that the Schrödinger equation is nearly separable in cylindrical coordinates, at least for $m=0$, odd-parity states at this (and higher) magnetic field strengths.

The agreement of length and velocity dipole matrix elements in Fig. 7 provides some evidence that two Landau channels adequately describe the final state. Still, the 10—15% discrepancy between the $\alpha=2$ matrix elements is most likely traceable to the omission of the $n=3$ Landau channel near $z=0$. The parameters of Figs. 5—7 permit a calculation of differential oscillator-strength distribution, through, e.g., Eqs. (30)—(40) of Ref. 26. The resulting df/dE are shown in Fig. 8 with both the length

TABLE II. Binding energies (a.u.) and oscillator strengths of the $m=0$, odd-parity bound states.

$E_0^{(0)}-E_N$		f_N		
Present	Ref. 10	Length	Velocity	Ref. 36
0.297 1	0.297 7	0.664	0.679	0.687
0.097 72	0.096 85	0.067 6	0.058 7	0.057 8
0.047 12	0.046 90	0.018 9	0.016 1	
0.027 61	0.027 52	0.007 91	0.006 71	

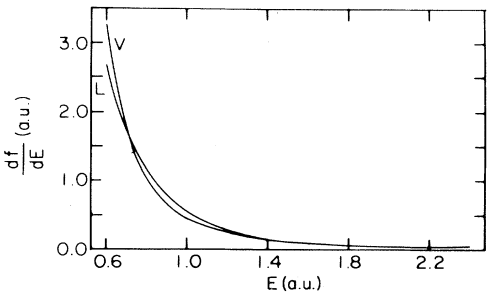

FIG. 4. Oscillator-strength distribution df/dE obtained when the hydrogen ground state is photoionized using photons linearly polarized along the field axis at $B=4.7\times10^9$ G. These are shown using both the length (L) and velocity (V) forms of the dipole matrix element. While the curves are shown continuously at $E<1$ a.u., in fact, the observed spectrum is then entirely discrete, with oscillator strengths given in Table II.

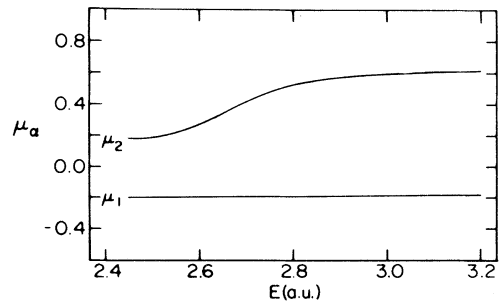

FIG. 5. Two eigenquantum defects μ_α are shown as a function of energy in the two-channel range near the first excited Landau threshold ($n=1$, $m=0$, odd parity) $E_1^{(0)}=3$ a.u. These are the eigenphaseshifts of the reaction matrix, divided by π.

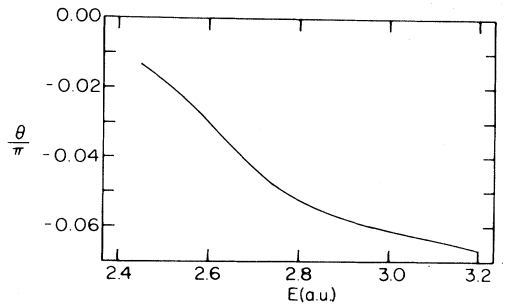

FIG. 6. Mixing angle θ/π for the final state is shown near $E_1^{(0)}=3$ a.u. This is the rotation angle needed to diagonalize the symmetric 2×2 reaction matrix. Notice the increasing importance of channel mixing as the threshold is approached from below.

and velocity results demonstrating the significant enhancement of oscillator strength which is produced by the autoionizing levels. These narrow states form a Rydberg series converging on the $n=1$ threshold at $E=3$ a.u.; the first four states are shown in Fig. 8. Above threshold, the oscillator strength becomes again a smooth continuum, and photoelectrons having two possible speeds v_z at $|z|\rightarrow\infty$ would be detected in an experiment. The data of Figs. 5 and 6 imply that near threshold the slower photoelectrons escape roughly four times as often as the faster photoelectrons.

IV. CONCLUSIONS

The qualitative and quantitative aspects of hydrogen photoionization in a strong magnetic field can clearly be

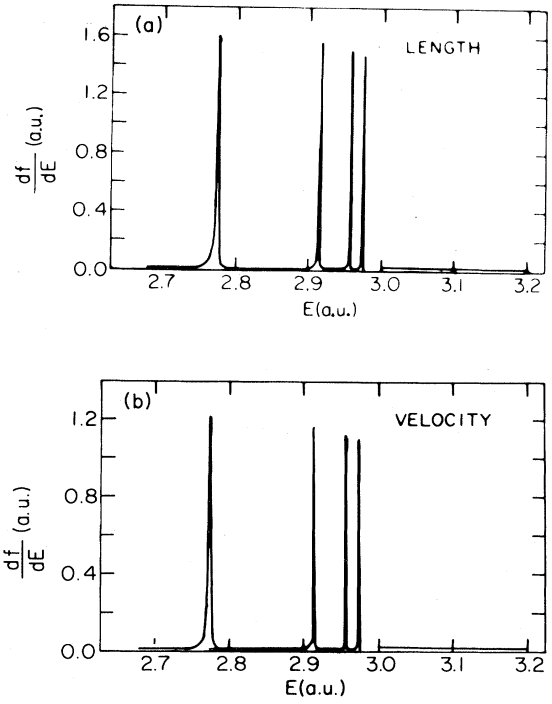

FIG. 8. Total photoionization oscillator strength of hydrogen at $B=4.7\times10^9$ G is given as a function of energy near the first excited Landau threshold $E_1^{(0)}=3$ a.u. Resonances form an infinite Rydberg series converging on this threshold, though only the lowest four are shown. Oscillator strength has a finite value at threshold and decreases slowly as the energy is increased further. It is shown using (a) length and (b) velocity forms of the dipole matrix element.

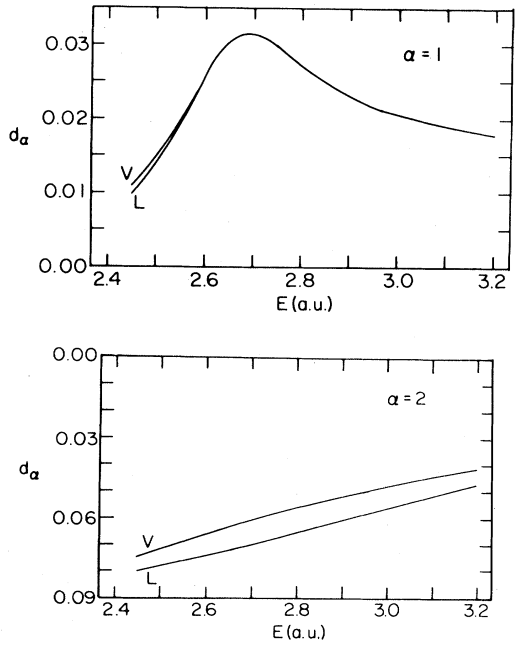

FIG. 7. Dipole matrix elements d_α calculated using either length (L) or velocity (V) forms.

treated realistically by the approach outlined in Sec. II. While the calculation presented has neither attempted high accuracy nor has it considered a range of magnetic field strengths, it has overcome the main difficulties to be encountered in such studies. A main conclusion reached is that for $B\geq4.7\times10^9$ G, the coupling between cylindrical channels is so small as to be perturbative, at least for $m=0$ and odd parity. This is probably not true of the $m=0$, even-parity channels. In this regard it may be interesting to survey the photoionization cross section at field strengths 10 to 100 times weaker, as the resonances will be significantly broader as the channel mixing (i.e., nonseparability) increases. For these lower field strengths another consequence of the increased channel interactions will be strong-level perturbations, which should necessitate a multichannel quantum-defect treatment even for the calculation of bound states. In addition, the lower field strengths are probably more relevant to astrophysical problems than is the field $B=4.7\times10^9$ G.

A second major result of the calculation is to provide further evidence that in any multichannel calculation the mixing with excited channels becomes important at considerably lower energies than the actual location of the first resonances in those channels. Comparison of Figs. 6

and 8 shows the channel mixing begins to grow above $E=2.5$ a.u., though the lowest resonance lies at $E=2.75$ a.u. Nonetheless, the onset of channel mixing does occur more smoothly as a function of energy here than was observed in Ref. 26. The circumstances determining this aspect are not well understood and remain a topic for future studies.

ACKNOWLEDGMENTS

Conversations with A.R.P. Rau have been extremely useful. I thank G. Wunner for providing results prior to publication and R. K. Nesbet for comments on an earlier version of this manuscript. This work was supported in part by the National Science Foundation.

[1]J. R. P. Angel, E. P. Borra, and J. D. Landstreet, Astrophys. J. Suppl. Ser. 45, 359 (1981).

[2]U. Fano, Phys. Rev. A 22, 2660 (1980).

[3]U. Fano and C. D. Lin, in *Atomic Physics IV,* edited by G. zu Putlitz, E. W. Weber, and A. Winnacker (Plenum, New York, 1975) p. 47; A. R. P. Rau, J. Phys. (Paris) Colloq. 43, C2-211 (1982).

[4]C. W. Clark and K. T. Taylor, Nature 292, 437 (1981).

[5]E. A. Solov'ev, Zh. Eksp. Teor. Fiz. 82, 1762 (1982) [Sov. Phys.—JETP 55, 1017 (1982)]; C. W. Clark, Phys. Rev. A 24, 605 (1981); D. R. Herrick, *ibid.* 26, 323 (1982); C. J. Goebel and T. W. Kirkman (unpublished).

[6]W. R. S. Garton and F. S. Tomkins, Astrophys. J. 158, 839 (1969).

[7]H. Friedrich and M. Chu, Phys. Rev. A 28, 1423 (1983).

[8]K. Onda, J. Phys. Soc. Jpn. 45, 216 (1978).

[9]R. H. Garstang, Rep. Prog. Phys. 40, 105 (1977).

[10]G. Wunner and H. Ruder, J. Phys. (Paris) Colloq. 43, C2-137 (1982).

[11]S. M. Kara and M. R. C. McDowell, J. Phys. B 14, 1719 (1981).

[12]G. Wunner, H. Ruder, H. Herold, and W. Schmitt (unpublished).

[13]M. J. Seaton, Proc. Phys. Soc. London 88, 801 (1966); Rep. Prog. Phys. 46, 167 (1983).

[14]U. Fano, J. Opt. Soc. Am. 65, 979 (1975).

[15]C. M. Lee and K. T. Lu, Phys. Rev. A 8, 1241 (1973).

[16]C. H. Greene, A. R. P. Rau, and U. Fano, Phys. Rev. A 26, 2441 (1982).

[17]C. H. Greene, Phys. Rev. A 22, 149 (1980).

[18]C. W. Clark, Phys. Rev. A 28, 83 (1983).

[19]C. M. Lee, Phys. Rev. A 10, 584 (1974); U. Fano and C. M. Lee, Phys. Rev. Lett. 31, 1573 (1973).

[20]W. Kohn, Phys. Rev. 74, 1763 (1948).

[21]J. L. Jackson, Phys. Rev. 83, 301 (1951).

[22]A. M. Lane and D. Robson, Phys. Rev. 178, 1715 (1969).

[23]J. E. Purcell, Phys. Rev. 185, 1279 (1969); R. A. Chatwin, Phys. Rev. C 2, 1167 (1970).

[24]R. S. Oberoi and R. K. Nesbet, Phys. Rev. A 8, 215 (1973); 9, 2804 (1974); R. K. Nesbet, *Variational Methods in Electron-Atom Scattering Theory* (Plenum, New York, 1980).

[25]H. Le Rouzo and G. Raseev (unpublished).

[26]C. H. Greene, Phys. Rev. A 23, 661 (1981).

[27]Ch. Jungen, in *Invited Papers in the Twelfth International Conference on the Physics of Electronic and Atomic Collisions,* edited by S. Datz (North-Holland, Amsterdam, 1982), p. 455.

[28]See, e.g., E. S. Chang and U. Fano, Phys. Rev. A 6, 173 (1972); also Ch. Jungen and O. Atabek, J. Chem. Phys. 66, 5584 (1977).

[29]P. G. Burke and W. D. Robb, Adv. At. Mol. Phys. 11, 143 (1975).

[30]J. H. Wilkinson, *The Algebraic Eigenvalue Problem,* (Oxford University Press, London, 1965).

[31]C. B. Moler and G. W. Stewart, SIAM J. Numer. Anal. 10, 241 (1973).

[32]The calculations in this paper have used subroutine EIGZF, which is found in the IMSL Library. It is a product of IMSL, Inc., 7500 Bellaire Blvd., 6th Floor, NBC Building, Houston Texas 77036-5085.

[33]Integrations in the z coordinate are generally performed over the interval $-\infty<z<\infty$. Since all nonzero integrals needed here involve integrands which are symmetric about $z=0$, they have all been evaluated instead over the range $0\leq z<\infty$ only. The $l=0$ Coulomb wave functions (f,g) of Ref. 17 are energy normalized over $0\leq z<\infty$, which permits their use without rescaling by the factor $1/\sqrt{2}$, as would be needed if (f,g) were to be energy normalized over $-\infty<z<\infty$.

[34]F. Scheid, *Theory and Problems of Numerical Analysis, Schaum's Outline Series* (McGraw-Hill, New York, 1968).

[35]See, e.g., A. F. Starace, in *Handbuch der Physik* edited by W. Mehlhorn (Springer, Berlin, 1982), Vol. XXXI.

[36]G. Wunner (private communication).

[37]H. A. Bethe and E. E. Salpeter, *Quantum Mechanics of One- or Two-Electron Atoms* (Springer, Berlin, 1957), p. 265.